
Article:
Wagg, D.J. (2005) Periodic sticking motion in a two-degree of freedom impact oscillator. International Journal of Non-Linear Mechanics, 40 (8). 1076 - 1087. ISSN: 0020-7462

https://doi.org/10.1016/j.ijnonlinmec.2005.03.002

International Journal of Non-Linear Mechanics 40 (2005) 1076–1087

Periodic sticking motion in a two-degree-of-freedom impact oscillator

D. J. Wagg*

Department of Mechanical Engineering, University of Bristol, Queens Building, University Walk, Bristol BS8 1TR, U.K.

May 3, 2013

Abstract

Periodic sticking motions can occur in vibro-impact systems for certain parameter ranges. When the coefficient of restitution is low (or zero), the range of periodic sticking motions can become large. In this work the dynamics of periodic sticking orbits with both zero and non-zero coefficient of restitution are considered. The dynamics of the periodic orbit is simulated as the forcing frequency of the system is varied. In particular the loci of Poincaré fixed points in the sticking plane are computed as the forcing frequency of the system is varied. For zero coefficient of restitution, the size of the sticking region for a particular choice of parameters appears to be maximized. We consider this idea by computing the sticking region for zero and non-zero coefficient of restitution values. It has been shown that periodic sticking orbits can bifurcate

*Author for correspondance:David.Wagg@bristol.ac.uk, Tel: +44 (117) 9289736, Fax : +44 (117) 929 4423

via the rising/multi-sliding bifurcation. In the final part of this paper we describe three types of post bifurcation behavior which occur for the zero coefficient of restitution case. This includes two types of rising bifurcation and a border orbit crossing event.

Keywords: Impact; 2DOF Oscillator; Periodic; Sticking; Multi-sliding

1 Introduction

In this paper periodic sticking motions which occur in the dynamics of a two-degree-of-freedom impact oscillator are considered. The impact oscillator consists of two masses, coupled with springs and dashpots, and the motion of both the masses is restricted by rigid constraints [1]. These type of systems can be used to model a range of physical applications mainly in mechanical engineering [2–9]. Many mathematical-numerical studies of these systems have been carried out, and particular interest has been focused on bifurcation behavior [10–16]. More general studies of multiple degree of freedom impact oscillators have also been carried out [17–22], but these focus primarily on a single impact constraint.

In mechanical systems with vibration and impact, chatter and sticking are phenomena which have been observed for a wide range of parameter values. Chatter and sticking in single degree of freedom impact oscillators has been studied in detail [23,24] and also noted to occur in two-degree-of-freedom systems, particularly for low forcing frequencies [25]. Vibro-impact systems exhibit a rich variety of periodic motions (see for example [26]), and periodic sticking motions can be found for particular parameter values in both single and multi-degree-of-freedom systems. Multi-degree-of-freedom systems with a single constraint have been studied by [27] and [25], where periodic sticking motions were observed for low forcing frequencies. In [1], periodic sticking motions were noted for a two-degree-of-freedom impact oscillator with two constraints, and it was shown how the entry boundary to the sticking region can be defined. The rising bifurcation discussed by [27] has been shown to be equivalent to the multi-sliding bifurcation [28], which occurs

in the study of nonsmooth systems [29–31].

In this paper we study the dynamics of periodic sticking motions which exist in a two-degree-of-freedom impact oscillator with motion constraints on both masses [1]. For low (or zero) coefficient of restitution, the range of periodic sticking motions becomes large. This is significant because the maximum extent of the sticking region should be defined for the zero case. This idea is considered by using a comparison of the sticking region obtained by simulating the dynamics of periodic sticking orbits with both zero and non-zero coefficient of restitution. Then the loci of Poincaré fixed points in the sticking plane are computed as the forcing frequency of the system is varied. Projections of these loci into the system state space indicate that the zero case does not define the largest region of sticking motions for the examples considered.

In the final part of this paper we consider the post bifurcation behavior following rising bifurcations in the zero coefficient of restitution case. We first illustrate the 'standard' rising bifurcation behavior described by [1, 27] and following this we describe one other example where the rising has a receding behavior. Finally we discuss an example were a sticking orbit passes through a border orbit [24], which defines the limiting extent of the sticking region.

2 Mathematical model

We consider a coupled two-degree-of-freedom system, which is shown schematically in figure 1. This system has already been described in detail in [1, 28]. The governing equations for the system away from impact can be expressed as

$$m_1\ddot{x}_1 + c_1\dot{x}_1 + c_2(\dot{x}_1 - \dot{x}_2) + k_1x_1 + k_2(x_1 - x_2) = f_1, \tag{1}$$

$$m_2\ddot{x}_2 + c_2(\dot{x}_2 - \dot{x}_1) + k_2(x_2 - x_1) = f_2, \tag{2}$$

where x_1 represents the displacement of mass m_1 and x_2 the displacement of mass m_2. The spring stiffnesses are given by k_1, k_2 and the damping constants by c_1, c_2 and the distance

to the motion constraints are given by s_1 and s_2 respectively. The harmonic forcing functions are $f_1 = A_1\cos(\Omega t)$ and $f_2 = A_2\cos(\Omega t)$. Equation 2 has a dual condition for free flight that $(x_i - s_i) < 0$ for $s_i > 0$ and $(x_i - s_i) > 0$ for $s_i < 0$ which can be written as $(x_i - s_i) \lessgtr 0, \quad \forall s_i \gtrless 0$, for $i = 1, 2$. We also assume that the distance between masses is large enough so that they do not impact with each other.

Equations (1) and (2) can be written in the nondimensionalized form

$$\begin{bmatrix} \mu_m & 0 \\ 0 & 1 \end{bmatrix} \begin{bmatrix} \ddot{\xi}_1 \\ \ddot{\xi}_2 \end{bmatrix} + \begin{bmatrix} 2\zeta_1\sqrt{\mu_m\mu_k} + 2\zeta_2 & -2\zeta_2 \\ -2\zeta_2 & 2\zeta_2 \end{bmatrix} \begin{bmatrix} \dot{\xi}_1 \\ \dot{\xi}_2 \end{bmatrix} + \begin{bmatrix} 1+\mu_k & -1 \\ -1 & 1 \end{bmatrix} \begin{bmatrix} \xi_1 \\ \xi_2 \end{bmatrix} = \begin{bmatrix} \tilde{f}_1 \\ \tilde{f}_2 \end{bmatrix} \tag{3}$$

where $\mu_m = m_1/m_2$, $\mu_k = k_1/k_2$, $\zeta_1 = c_1/(2m_1\varpi_{n1})$, $\zeta_2 = c_2/(2m_2\varpi_{n2})$, $\varpi_{n1} = \sqrt{k_1/m_1}$, $\varpi_{n2} = \sqrt{k_2/m_2}$, $\omega = \Omega/\varpi_{n2}$, $\tilde{f}_1 = P_1\cos(\omega\tau)$, $\tilde{f}_1 = P_2\cos(\omega\tau)$, $P_1 = A_1/(k_2x_c)$, $P_2 = A_2/(k_2x_c)$, $\tau = \varpi_{n2}t$ and $\xi = x/x_c$. The nondimensional variable ξ is achieved by dividing displacement, x, by a constant displacement x_c. This choice is arbitrary, and therefore we will assume that $x_c = 1$, such that the nondimensional distances to the motion constraints are $\sigma_1 = s_1/x_c$ and $\sigma_2 = s_2/x_c$. The nondimensional phase, ϕ, is defined as $\phi = \tau \bmod 2\pi/\omega$.

The parameter values have been selected as $m_1 = m_2 = k_1 = k_2 = 1$ and $c_1 = c_2 = 0.1$ which means that in the nondimensionalized case $\mu_m = \mu_k = \varpi_{n1} = \varpi_{n2} = 1$ and $\zeta_1 = \zeta_2 = \zeta$. These specific parameters were chosen to give a simple relationship between the natural frequencies and the system eigenvalues, and the damping value is chosen to represent a physically realistic choice for a mechanical spring-mass-damper system. In this case, equation (3) simplifies to

$$\begin{bmatrix} \ddot{\xi}_1 \\ \ddot{\xi}_2 \end{bmatrix} + 2\zeta \begin{bmatrix} 2 & -1 \\ -1 & 1 \end{bmatrix} \begin{bmatrix} \dot{\xi}_1 \\ \dot{\xi}_2 \end{bmatrix} + \begin{bmatrix} 2 & -1 \\ -1 & 1 \end{bmatrix} \begin{bmatrix} \xi_1 \\ \xi_2 \end{bmatrix} = \begin{bmatrix} P_1\cos(\omega\tau) \\ P_2\cos(\omega\tau) \end{bmatrix}. \tag{4}$$

The natural frequencies of the nondimensional system are given by $\sqrt{\lambda_j}$ for $j = 1, 2$

where λ_j are the eigenvalues of the 2×2 coupling matrix

$$[E] = \begin{bmatrix} 2 & -1 \\ -1 & 1 \end{bmatrix}. \tag{5}$$

The corresponding normalized eigenvectors ν_j can be used to construct a orthogonal modal matrix $[\Psi] = [\{\nu_1\}, \{\nu_2\}]$. We can then transform equation (4) into a modal form by defining modal coordinates $q = \{q_1, q_2\}^T$, such that $\xi = [\Psi]q$ and

$$[I]\ddot{q} + 2\zeta\Lambda\dot{q} + [\Lambda]q = [\Psi]^T\hat{f}(t) \tag{6}$$

where $[\Lambda] = [\Psi]^T[E][\Psi]$ is the diagonal matrix of the eigenvalues, λ_j, $j = 1, 2$ and $\hat{f}(t) = [P_1\cos(\omega\tau), P_2\cos(\omega\tau)]^T$.

In this modal formulation, we define the vector $\psi_i = [\Psi_{i1}, \Psi_{i2}]$, such that an impact occurs when $\psi_i q = \sigma_i$, $i = 1, 2$. Hence equation (6) is valid only for $(\psi_i q - \sigma_i) \lesseqgtr 0, \quad \forall\sigma_i \gtreqless 0$, which is equivalent to the condition that $(x_i - s_i) \lesseqgtr 0, \quad \forall s_i \gtreqless 0$ for the ith impacting mass. For this system there are two modal impact vectors, $\psi_1 = [\Psi_{11}, \Psi_{12}]$ and $\psi_2 = [\Psi_{21}, \Psi_{22}]$, such that at impact $\psi_1 q = \sigma_1$ and $\psi_2 q = \sigma_2$, where $q = [q_1, q_2]^T$.

Equation (6) for each mode (with $P_2 = 0$) is given by

$$\ddot{q_j} + 2\zeta_j\lambda_j\dot{q_j} + \lambda_j q_j = \Psi_{1i}P_1\cos(\omega\tau), \quad j = 1, 2. \tag{7}$$

Equation (7) has a well known exact solution for under-damped oscillations $0 < \zeta_j < 1$ [32], such that for each mode exact solutions can be found between impacts [1]. We consider only the under-damped case as this is the case of most interest for mechanical systems. For the numerical simulations in this paper we set the forcing amplitudes as $P_2 = 0$ and $P_1 = 0.5$ and take initial conditions $q_1(t_0) = q_2(t_0) = \dot{q}_1(t_0) = \dot{q}_1(t_0) = t_0 = 0$.

When $(\xi_i - \sigma_i) = 0$ for $i = 1, 2$ an impact occurs which is modelled using an instantaneous coefficient of restitution rule [33] . For single impacts the coefficient of restitution rule is $\dot{x}_i(t_+) = -r\dot{x}_i(t_-)$, where, t_- is the time just before impact, t_+ is the time just

after impact and r is the coefficient of restitution with a value in the range $r \in [0,1]$. In matrix form the coefficient of restitution rule can be written as $\dot{\xi}(t_+) = [R_k]\dot{\xi}(t_-)$ where for the system being considered there are three different cases for the $[R_k]$ matrices

$$[R_1] = \begin{bmatrix} -r & 0 \\ 0 & 1 \end{bmatrix}, \quad [R_2] = \begin{bmatrix} 1 & 0 \\ 0 & -r \end{bmatrix}, \quad [R_3] = \begin{bmatrix} -r & 0 \\ 0 & -r \end{bmatrix}. \tag{8}$$

corresponding to mass 1 impacting, mass 2 impacting and simultaneous impact of both masses.

In modal form the coefficient of restitution rule becomes $[\Psi]\dot{q}(\tau_+) = [R_k][\Psi]\dot{q}(\tau_-)$, which leads to the relation for the modal velocities after impact of $\dot{q}(\tau_+) = [\hat{R}_k]\dot{q}(\tau_-)$, where $[\hat{R}_k] = [\Psi]^{-1}[R_k][\Psi]$ is the set of matrices which represents a linear transform of modal velocities just before impact to modal velocities just after impact for the 3 possible impact cases [1].

2.1 Sticking solutions

For this system there are two possible sticking regimes; when $\xi_1 = \sigma_1$ and when $\xi_2 = \sigma_2$. Each regime has a reduced set of governing equations with explicit solutions [1]. It is also possible to have a dual sticking regime when both $\xi_1 = \sigma_1$ and $\xi_2 = \sigma_2$ simultaneously, with the result that there are no dynamics in the system.

In the case where mass 1 sticks $\xi_1 = \sigma_1$ and $\dot{\xi}_1 = 0$, and the equations of motion reduce to a single equation

$$\ddot{\xi}_2 + 2\zeta\dot{\xi}_2 + \xi_2 = \sigma_1. \tag{9}$$

The condition for the mass being held in place during sticking is related to the force on the mass. The equivalent nondimensional release expression is given by

$$\mathcal{F}_2 = 2\zeta\dot{\xi}_2 + \xi_2 - 2\sigma_1 + P_1\cos(\omega\tau). \tag{10}$$

The forcing term $P_2 = 0$ in equation 9, but P_1 occurs in the release expression, so this case is referred to as the forced sticking case. The sticking phase ends when $\mathcal{F}_2$ becomes

zero and changes sign at which time $\tau = \tau_f$. Equation (9) has the exact solution

$$\xi_2 = e^{-\zeta(\tau-\tau_s)}(C_1 \cos[\sqrt{1-\zeta^2}(\tau-\tau_s)] + C_2 \sin[\sqrt{1-\zeta^2}(\tau-\tau_s)]) + \sigma_1. \tag{11}$$

At the start of the sticking period $\tau_s = \tau$ and the constants C_1 and C_2 are found using the initial conditions for ξ_2 and $\dot{\xi}_2$ when $\xi_1(\tau_s) = \sigma_1$ and $\dot{\xi}_1(\tau_s) = 0$ [1].

In the case $\xi_2 = \sigma_2$ and $\dot{\xi}_2 = 0$, the reduced equation of motion is given by

$$\ddot{\xi}_1 + 2\zeta\dot{\xi}_1 + 2\xi_1 - \sigma_2 = P_1 \cos(\omega t). \tag{12}$$

The release condition is governed by

$$\mathcal{F}_1 = \zeta\dot{\xi}_1 + \xi_1 - \sigma_2. \tag{13}$$

This is therefore referred to as the unforced sticking case.

Equation (12) has the exact solution

$$\xi_1 = e^{-2\zeta(\tau-\tau_s)}(C_1 \cos(2\sqrt{1-\zeta^2}(\tau-\tau_s)) + C_2 \sin(2\sqrt{1-\zeta^2}(\tau-\tau_s))) + C_3 \cos(\omega t - \varphi) + \sigma_2/2, \tag{14}$$

where $\varphi = \arctan((4\zeta\omega)(2-\omega^2))$.

The initial conditions for both reduced equations can be taken directly from the appropriate values of ξ_i and $\dot{\xi}_i$ immediately prior to a sticking phase. These initial conditions allow the computation the constants C_1, C_2 prior to the beginning of the next phase of motion, and C_3 is found as part of the particular solution [1].

3 Periodic sticking motion

An example of the type of periodic sticking orbit which will be considered in this paper is shown schematically in figure 2. In this example $r = 0$ and sticking occurs for mass 1 between A and A', and for mass 2 between B and B'. One complete period occurs between points A and C. From A to A' mass 1 is stuck and mass 2 is in free flight. Then

from A' to B both masses are in free flight, followed by a second sticking regime from B to B' where mass 2 is stuck and mass 1 is in free flight. Finally both masses are in free flight between B' and C. The period of (nondimensional) time spent sticking is T_{si} for $i = 1, 2$ and for periodic sticking orbits the proportion of the whole period spent sticking is $p_i = T_{si}/T$, where $T = 2\pi/\omega$ so that $p_i = T_{si}\omega/2\pi$.

The change from free motion of both masses to one mass sticking represents a reduction in the degree of freedom of the system from 2 to 1. For the example in figure 2 this reduction from 2 to 1 occurs at points A and B. Similarly there is an increase in degree of freedom from 1 to 2 at points A' and B'.

The two-degree-of-freedom system has a parameter set $\mu = \{\zeta, P_1, P_2, \omega, \sigma_1, \sigma_2, r\}$. For any particular choice of these parameter values there could typically be regions of non-impacting behavior, vibro-impacting behavior, chatter and sticking [25]. We will assume that $P_2 = 0$, and that $\zeta, P_1, \omega, \sigma_1, \sigma_2$ have suitable constant values such that for a range of excitation frequencies ω, vibro-impacting motions, chatter and sticking occur. For such a choice of parameters, the coefficient of restitution, r, will then define the extent of the potential sticking region, S, for periodic sticking orbits.

For $r = 0$, the impacts are completely plastic, and sticking will generally occur after every impact — in section 4.1 we show an exception to this where impact occurs without sticking. For $r \neq 0$, sticking will only occur after a complete chatter sequence [23], and as a result sticking orbits will occur for lower excitation frequencies — because this allows chatter to become complete. As $r \to 1$ impacts tend towards being perfectly elastic and sticking orbits will not appear even for low excitation frequencies. A numerical example is shown in Figure 3, where we compare two time series. In Figure 3 (a), the coefficient of restitution is $r = 0.7$, and in Figure 3 (b), the coefficient of restitution is $r = 0.0$. It is clear that for the $r = 0.0$ the sticking proportions of the periodic orbit, p_1, p_2 are at their maximum values for all the other parameters in μ fixed.

3.1 Classifying periodic sticking orbits

Periodic impacting orbits are usually classified by the number of forcing periods, n, and the number of impacts, m, which occur during one period of the motion, denoted $P(n, m)$ [34]. Periodic orbits with sticking have an infinite number of instantaneous impacts during one period of motion [23], so every periodic sticking orbit is classified $P(n, \infty)$. With the understanding of multi-sliding bifurcations [29–31], and how they occur in impacting systems [28], there is a further distinction which can be made for periodic sticking orbits — the number (and duration) of the sticking phase(s). For example, if k is the number of sticking phases per period we could classify the orbit using $P(n, \infty, k)$. A more detailed classification would include the proportion of the period spent sticking, $p = [p_1, p_2]$, such that $P(n, \infty, k, p)$. In fact the majority of periodic sticking orbits considered in this work are $P(1, \infty, 1)$. In the case where a periodic motion occurs with a sticking phase and an additional number of separate impacts we use the notation $P(n, \infty + m, k)$, an example of this is discussed in section 4.1.

3.2 The sticking region

Sticking behavior in vibro-impact systems is analogous to sliding behavior in some electrical systems [29], as discussed in [28]. For studying the behavior of sticking orbits in general, it is useful to define the region in the system phase space where these orbits exist. The sticking/sliding region(s) consists of a manifold(s) within the system state space on which the sticking/sliding orbits exist. These sticking/sliding orbits are then (usually) restricted to some region on the manifold by conditions which define the entry (start of sliding) and exit (end of sliding) of the orbit from the manifold. For some systems [29] it is possible to define the manifold and the entry and exit boundaries explicitly. For vibro-impact systems is has been pointed out that only the manifold and exit boundary can be defined explicitly [1].

For the system studied here there are two manifolds in the system state space on which sticking can take place. These are defined by the impact conditions of the system such that if $\xi = \{\xi_1, \xi_2, \dot{\xi}_1, \dot{\xi}_2, \phi\}^T$ is the state vector, then the system state space can be defined as $G = \{\xi \in \mathbb{R}^4 \times \phi : \xi_1 \leq \sigma_1, \xi_2 \leq \sigma_2\}$. Then the two impact manifolds are defined as $\Sigma_1 = \{\xi \in \mathbb{R}^4 \times \phi : \xi_1 = \sigma_1, \dot{\xi}_1 = 0\}$ and $\Sigma_2 = \{\xi \in \mathbb{R}^4 \times \phi : \xi_2 = \sigma_2, \dot{\xi}_2 = 0\}$. On each impact manifold, Σ_i, a corresponding sticking region S_i exists for $i = 1, 2$. The condition for a sticking orbit to leave the sticking region S_i is given by the equations for $\mathcal{F}_i = 0$, for $i = 1, 2$ — equations 10 and 13. Therefore we can analytically define the exit boundary of each sticking region ∂S_i, using the conditions for $\mathcal{F}_i = 0$, for $i = 1, 2$ in equations 10 and 13.

Although there is no way of analytically defining the entry boundary of the sticking regions, it would appear from Figure 3 that the entry boundary could be defined by the point of first sticking when $r = 0$. i.e. the maximum possible extent of the sticking region occurs when no chatter precedes the sticking. Therefore to test whether the $r = 0$ case does define the maximum possible extent of the sticking region, the loci of the first sticking points for mass 2 sticking (point B in Figure 2) have been computed as the forcing frequency is varied. Because mass 2 is sticking, the state variables which will define the sticking orbit are ξ_1, $\dot{\xi}_1$ and ϕ, and we will plot these values at the point where mass 2 first sticks i.e. the entry point into the sticking region. For the $r = 0$ case the bifurcation diagrams showing the amplitude of ξ_1 and ϕ at the first sticking point as ω is varied through the range 0.1–2.5 are shown in Figure 4 (a) and (c) respectively. As a comparison we have shown the same plots for the $r = 0.7$ case in Figure 4 (b) and (d), from which we note that sticking exists for a much larger range of ω values in the $r = 0$ case. Note also that there are some nonsmooth jumps in the variation of ϕ with ω shown in Figures 4 (c) and (d). This is explained by observing the the modulo value, $2\pi/\omega$, which is plotted as a dashed line in Figures 4 (c) and (d). For both cases shown in Figure

4, $r = 0$ (Figure 4 (c)) and $r = 0.7$ (Figure 4 (d)), the loci begins at a value below the modulo value. However in both cases, as ω is increased, the loci eventually intersect with the modulo line such that the phase value becomes zero. This explains the jumps of the loci in Figure 4 (c) and (d), at $\omega \approx 0.75$ for Figure 4 (c) and $\omega \approx 0.21$ in Figure 4 (d). This also accounts for the division of the loci into two sections in Figures 5 (c) and (d).

As ω is varied the first sticking points defined by ξ_1, $\dot{\xi}_1$ and ϕ describe a locus in $\mathbb{R}^3$. In Figure 5 (a) the projection of this locus into the $\xi_1, \dot{\xi}_1$ plane is shown, and in Figure 5 (c) the projection into the $\phi, \dot{\xi}_1$ plane is shown. These loci define the entry into the sticking region, and the exit boundary ∂S_1 is marked as a dashed line in Figure 5 (a).

By comparing the zero and non-zero case, we can see that the loci have a particularly complex structure when projected into the $\xi_1, \dot{\xi}_1$ plane, Figures 5 (a) and (b). It is also clear that the $r = 0$ loci does not encompass the entire region occupied by the $r = 0.7$ loci for the $\xi_1, \dot{\xi}_1$ projection. However the explanation of this is apparent from the time series in Figure 3, where it can be seen that due to the time at which the sticking starts, the magnitude of ξ_1 value is greater for the $r = 0.7$ case than for the $r = 0$ case. This can also be seen by comparing Figures 4 (a) and (b) where the value of ξ_1 at the first sticking point is plotted against ω. For the $\phi, \dot{\xi}_1$ projections shown in Figures 5 (c) and (d), it can be seen that the $r = 0$ loci does not encompass the entire region occupied by the $r = 0.7$ loci, but it does have higher values — indicating a stronger possibility for defining a bound on the region S_1.

It is interesting to note that as the system parameter ω is varied smoothly, the resulting first sticking loci contain several discontinuities — nonsmooth points and discontinuous jumps. Apart from phase transitions, these points represent nonsmooth changes (bifurcations) in the dynamics of the periodic orbits, and will be discussed in section 4.

4 Sliding bifurcations

The sliding orbits in electrical systems have been shown to exhibit particular types of *sliding bifurcations* under parameter variation [29]. There are four types of sliding bifurcation which can occur [30], for which the normal form mappings have been derived [31]. A *multi-sliding* bifurcation is one of the four cases, which occurs in the systems studied by [29–31], and is the most significant for our current study. Previous physical examples of the multi-sliding bifurcation have been studied in models of relay feedback systems [29] and friction oscillators [35].

In addition to multi-sliding, in the case of $r = 0$, the system will normally have a grazing-sliding bifurcation (in this example grazing followed by sticking) each time a grazing event occurs. This is similar to the grazing-sliding in the friction oscillator example studied by [35], but will not be considered in detail here.

4.1 Three examples of post bifurcation behavior

The multi-sliding (or rising) bifurcation occurs when a sliding (sticking) orbit touches the boundary of the sliding (sticking) region S_i [27, 28]. Physically this means that the force holding the mass against the constraint becomes zero, and as the bifurcation parameter continues to vary, the mass lifts off (or rises) from the the constraint. This results in a sudden reduction in sticking time [27, 28].

In this subsection we look a three different types of post bifurcation behavior which relate to observations of the behavior of the first sticking loci shown in Figures 4 and 5 for the $r = 0$ case. All three examples are for mass 1 sticking. The first example is shown in Figure 6, and occurs close to $\omega = 0.254$. In Figure 6 (a) and (b) we see that a rising has occurred some where near the middle of the sticking phase. As ω increases the rise propagates towards the release point for the mass, Figure 6 (c) and (d). The result is that the single sticking region is divided into two parts. So the periodic sticking orbit

goes from $P(1,\infty,1) \rightarrow P(1,\infty,2)$. However the sticking phase following the rise quickly decreases until a limit point, where it becomes a single point (like grazing) just before the mass lifts off — Figure 6 (d) then (f). This type of post multi-sliding behavior will be called the standard case, and has been discussed by [27, 28].

A second example of post multi-sliding behavior is shown in Figure 7, and occurs close to $\omega = 0.475$. In this case the rise is very close to the first sticking point. As with the standard case, the periodic sticking orbit goes from $P(1,\infty,1) \rightarrow P(1,\infty,2)$, but one of the new sticking phases is very small. The post multi-sliding behavior is then that the rise becomes larger in amplitude, before reaching a maximum and then declining until $P(1,\infty,2) \rightarrow P(1,\infty,1)$ through a reverse multi-sliding event. Note, this event can be seen in Figure 4 (a) as a series of points below the main loci close to $\omega = 0.475$. This is called the receding multi-sliding case.

The last example, shown in Figure 8, occurs for frequency values close to $\omega = 0.7$. In this example the sliding orbit passes through what has now been termed a border orbit — the orbit on which the sticking zone shrinks to zero [24]. In this case, the mass first impacts without sticking, and then impacts with a sticking phase, classified as a $P(1,1+\infty,1)$ periodic orbit. It is worth noting that in this type of multi-mass system it is possible for an impact to occur without sticking even for the $r = 0$ case. This can be seen from equation 10, which is the release condition for when mass 1 is sticking. When an impact occurs, Equation 10 must have the same sign as the constraint distance (negative in this case) for sticking to occur. In effect, equation 10 is the nondimensional equivalent of the force holding the mass against the constraint [1] — if the mass impacts and the force is acting *away* from the constraint, then no sticking will occur. It is clear that this force is dependent on the displacement and velocity of mass two and the external forcing. For example, computing the values of $\mathcal{F}_2$ for Figure 8 (b) ($\omega = 0.85$), at the first impact ($\tau = 964.12$) $\mathcal{F}_2 = 0.202$, so no sticking occurs. At the second impact ($\tau = 965.65$)

$\mathcal{F}_2 = -0.1594$, so sticking does occurs.

As ω is increased, the sticking phase (for mass 1) reduces to zero, until the border orbit is reached Figure 8 (c). Beyond this, mass 1 has no sticking phase (although mass 2 continues to stick until a border orbit close to $\omega = 1.4$ — Figure 4 (a)). The border orbit event for mass 1 has a clear effect on the sticking values for mass 2 which can be seen clearly in Figure 4 (a) as the discontinuity close to $\omega = 0.9$. This effect can also be seen clearly as a sharp discontinuity in Figure 5 (a) and (c). So in the border orbit crossing the periodic orbit makes the transition from $P(1, 1+\infty, 1) \to P(1, 1)$ — sticking periodic orbit to impacting periodic orbit.

5 Conclusions

In this paper we have examined the behavior of periodic sticking orbits which occur in a two-degree-of-freedom impact oscillator. For these periodic sticking orbits, two cases have been considered, one with $r = 0.7$ and the other with $r = 0$. For each case we have computed the loci of first sticking points in the sticking region — as forcing frequency is varied — demonstrating the complex nature of the entry boundary for this region. The projections of the sticking region into the $\xi_1, \dot{\xi}_1$, and $\phi, \dot{\xi}_1$ planes indicated that the condition $r = 0$ did not bound the sticking region completely — although in the $\phi, \dot{\xi}_1$ plane the first sticking loci provided a partial boundary to the region.

Plots of the loci of first sticking points against the bifurcation parameter (forcing frequency) showed clear nonsmooth jumps and discontinuities. Three of these nonsmooth events have been discussed in more detail, including two types of multi-sliding bifurcation and a border orbit crossing. The discovery of multi-sliding bifurcations and border orbit crossing in models of mechanical and electrical systems is a very recent addition to the literature on this subject. In this paper we have shown, by example, how border orbit crossing events manifest themselves. We have also shown that multi-sliding bifurcations

can have two distinct types of post bifurcation behavior — the standard case and the receding case involving a reverse multi-sliding event.

6 Acknowledgements

This work was supported as part of an Advanced Research Fellowship from the EPSRC. The author would like to thank Piotr Kowalczyk for constructive comments regarding this work.

References

[1] D. J. Wagg and S. R. Bishop. Dynamics of a two degree of freedom vibro-impact system with multiple motion limiting constraints. *International Journal of Bifurcation and Chaos*, 14(1):119–140, 2004.

[2] S. F. Masri. Theory of the dynamic vibration neutraliser with motion-limiting stops. *Transactions of the American Society of Mechanical Engineers, Journal of Applied Mechanics*, 39:563–568, 1972.

[3] F. C. Moon and S. W. Shaw. Chaotic vibrations of a beam with non-linear boundary conditions. *International Journal of Non-Linear Mechanics*, 18(6):465–477, 1983.

[4] S. Chatterjee, A. K. Mallik, and A. Ghosh. On impact dampers for non-linear vibrating systems. *Journal of Sound and Vibration*, 187(3):403–420, 1995.

[5] C. N. Bapat. The general motion of an inclined impact damper with friction. *Journal of Sound and Vibration*, 184(3):417–427, 1995.

[6] B. Blazejczyk-Okolewska. Analysis of an impact damper of vibrations. *Chaos, Solitions and Fractals*, 12:1983–1988, 2001.

[7] S. E. Semercigil, F. Collette, and D Huyni. Experiments with tuned absorber — impact damper combination. *Journal of Sound and Vibration*, 256(1):179–188, 2002.

[8] M. F. A. Azeez and A. F. Vakakis. Numerical and experimental analysis of a continuous overhung rotor undergoing vibro-impacts. *International Journal of Non-linear Mechanics*, 34:415–435, 1999.

[9] P. Metallidis and S. Natsiavas. Vibration of a continuous system with clearance and motion constraints. *International Journal of Non-linear Mechanics*, 35:675–690, 2000.

[10] J. Shaw and S. W. Shaw. The onset of chaos in a two-degree of freedom impacting system. *Journal of Applied Mechanics*, 56:168–174, 1989.

[11] G. W. Luo and J. H. Xie. Hopf bifurcation of a two-degree-of-freedom vibro-impact system. *Journal of Sound and Vibration*, 213:391–408, 1998.

[12] G-L Wen. Codimension-2 hopf bifurcation of a two-degree-of-freedom vibro-impact system. *Journal of Sound and Vibration*, 242(3):475–485, 2001.

[13] G. W. Luo and J. H. Xie. Hopf bifurcations and chaos of a two-degree-of-freedom vibro-impact system in two strong resonance cases. *Non-linear Mechanics*, 37:19–34, 2002.

[14] S. J. Hogan and M. E. Homer. Graph theory and piecewise smooth dynamical systems of arbitary dimension. *Chaos, Solitons & Fractals*, 10(11):1869–1880, 1999.

[15] S. Lenci and G. Rega. Regular nonlinear dynamics and bifurcations of an impacting system under general periodic excitation. *Nonlinear Dynamics*, 34:249–268, 2004.

[16] A. X. C. N. Valente, N. H. McClamroch, and I. Mezic. Hybrid dynamics of two

coupled oscillators that can impact a fixed stop. *International Journal of Non-Linear Mechanics*, 38:677–689, 2003.

[17] S. Theodossiades and S. Natsiavas. Periodic and chaotic dynamics of motor-driven gear-pair system with backlash. *Chaos, Solitons and Fractals*, 12:2427–2440, 2001.

[18] J. P. Cusumano and B-Y. Bai. Period-infinity periodic motions, chaos and spatial coherence in a 10 degree of freedom impact oscillator. *Chaos, Solitons and Fractals*, 3:515–536, 1993.

[19] M. M. Nigm and A. A. Shabana. Effect of an impact damper on a multi-degree of freedom system. *Journal Of Sound and Vibration*, 89(4):541–557, 1983.

[20] F. Pfeiffer and C. Glocker. *Multibody dynamics with unilateral contacts*. John Wiley, 1996.

[21] S. Natsiavas. Dynamics of multiple-degree-of-freedom oscillators with colliding components. *Journal of Sound and Vibration*, 165(3):439–453, 1993.

[22] D. Pun, S. L. Lua, S. S. Law, and D. Q. Cao. Forced vibration of a multidegree impact oscillator. *Journal of Sound and Vibration*, 213(3):447–466, 1998.

[23] C. J. Budd and F. Dux. Chattering and related behaviour in impact oscillators. *Philosophical Transactions of the Royal Society of London A*, 347:365–389, 1994.

[24] A. B. Nordmark and R. E. M. Kisitu. On chattering bifurcations in 1dof impact oscillator models. Preprint Royal Institute of Technology, Sweden, 2003.

[25] D. J. Wagg and S. R. Bishop. Chatter, sticking and chaotic impacting motion in a two-degree of freedom impact oscillator. *International Journal of Bifurcation and Chaos*, 11(1):57–71, 2001.

[26] C. N. Bapat. Periodic motions of an impact oscillator. *Journal of Sound and Vibration*, 209(1):43–60, 1998.

[27] C. Toulemonde and C Gontier. Sticking motions of impact oscillators. *European Journal of Mechanics A:Solids*, 17(2):339–366, 1998.

[28] D. J. Wagg. Rising phenomena and the multi-sliding bifurcation in a two-degree of freedom impact oscillator. Submitted to Chaos, Solitions and Fractals, 2003.

[29] M. Di Bernardo, K. H. Johansson, and F. Vasca. Self-oscillations and sliding in relay feedback systems:symmetry and bifurcations. *International Journal of Bifurcation and Chaos*, 4(11):1121–1140, 2001.

[30] P. Kowalczyk and M. di Bernardo. On a novel class of bifurcations in hybrid dynamical systems. In *Lecture Notes in Computer Science*, number 2034, pages 361–374, 2001.

[31] M. Di Bernardo, P. Kowalczyk, and A. Nordmark. Bifurcations of dynamical systems with sliding: derivation of normal-form mappings. *Physica D*, 170:175–205, 2002.

[32] S. P. Timoshenko. *Vibration problems in engineering*. Van Nostrand, 1937.

[33] J. M. T. Thompson and H. B. Stewart. *Nonlinear dynamics and chaos*. John Wiley: Chichester, 2002.

[34] S. W. Shaw and P. J. Holmes. A periodically forced piecewise linear oscillator. *Journal of Sound and Vibration*, 90(1):129–155, 1983.

[35] M. Di Bernardo, P. Kowalczyk, and A. Nordmark. Sliding bifurcations: A novel mechanism for the onset of chaos in dry friction oscillators. *International Journal of Bifurcation and Chaos*, 13(10):2935–2948, 2003.

Figure Captions

- Figure 1 Schematic representation of an N degree of freedom impact oscillator with multiple motion limiting constraints.

- Figure 2 Schematic diagram of a periodic sticking orbit. Sticking occurs between A to A' and B to B'. Solid line mass 1, dashed line mass 2.

- Figure 3 Time series showing; (a) $r = 0.7$ and (b) $r = 0$. The maximum potential sticking region occurs when $r = 0$. Parameters $\zeta = 0.05, P_1 = 0.5, \omega = 0.4, \sigma_1 = -0.3, \sigma_2 = 0.1$.

- Figure 4 First sticking loci as ω is varied: (a) and (b) values of ξ_1 at the point when mass 2 sticks to the constraint. (c) and (d) corresponding values of ϕ. (a) and (c) $r = 0$, (b) and (d) $r = 0.7$. Parameters $\zeta = 0.05, P_1 = 0.5, \sigma_1 = -0.3, \sigma_2 = 0.1$

- Figure 5 First sticking loci as ω is varied from 0.1 to 2.5: (a) and (b) projected onto the $\dot{\xi}, \xi$ plane. (c) and (d) projection onto the $\dot{\xi}, \phi$ plane. (a) and (c) $r = 0.0$, (b) and (d) $r = 0.7$. The dashed line in (a) and (b) denotes the boundary of the sticking region ∂S where the constraining force drops to zero, and the mass is released from sticking. Parameters $\zeta = 0.05, P_1 = 0.5, \sigma_1 = -0.3, \sigma_2 = 0.1$

- Figure 6 Rising bifurcation sequence 1: Solid line is mass 1, dashed line mass 2. Parameters $\zeta = 0.05, P_1 = 0.5, \sigma_1 = -0.3, \sigma_2 = 0.1$, $r = 0$; (a) and (b) $\omega = 0.254$, (c) and (d) $\omega = 0.26$, (e) and (f) $\omega = 0.265$.

- Figure 7 Rising bifurcation sequence 2: Solid line is mass 1, crosses are computation points. Parameters $\zeta = 0.05, P_1 = 0.5, \sigma_1 = -0.3, \sigma_2 = 0.1, r = 0, \omega = 0.469 - 0.505$.

- Figure 8 Border orbit crossing: Solid line is mass 1. Parameters $\zeta = 0.05, P_1 = 0.5, \sigma_1 = -0.3, \sigma_2 = 0.1$, $r = 0$, $\omega = 0.7 - 0.91$.

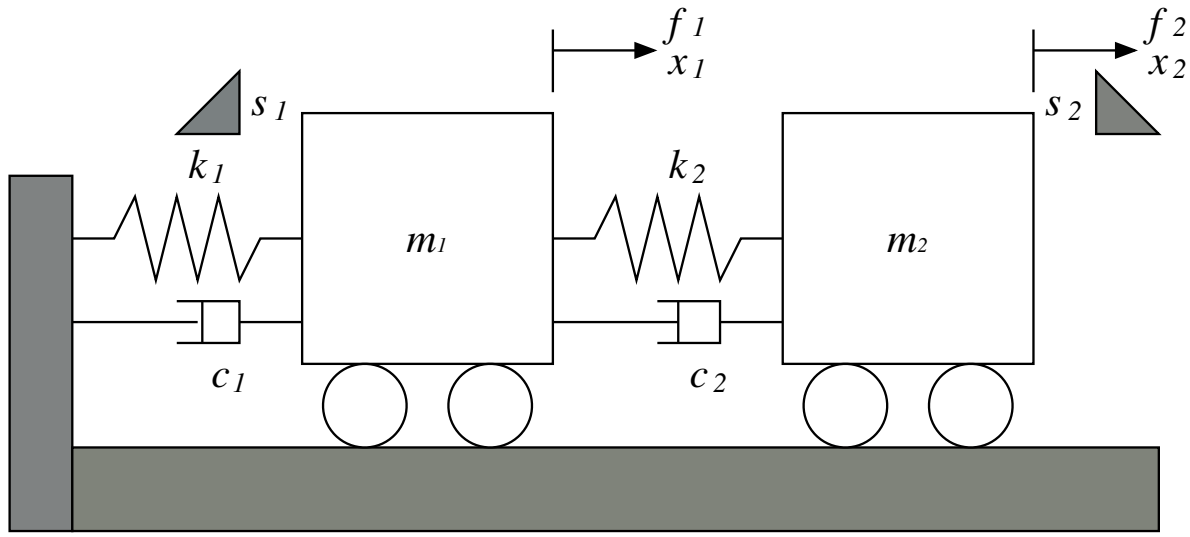

Figure 1:

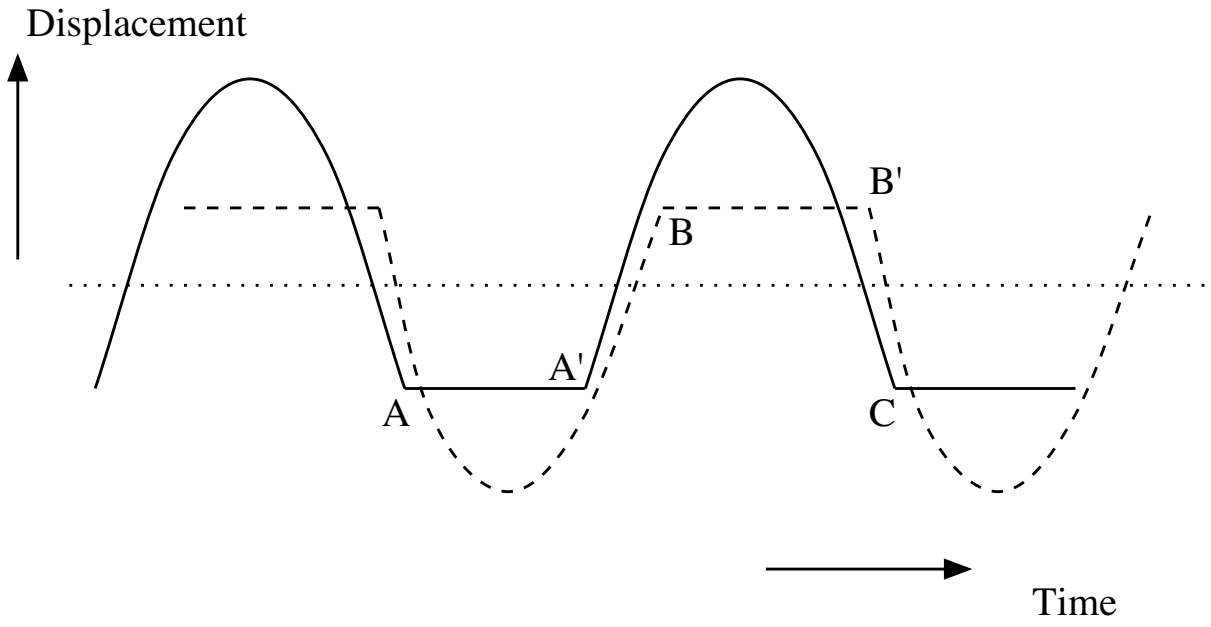

Figure 2:

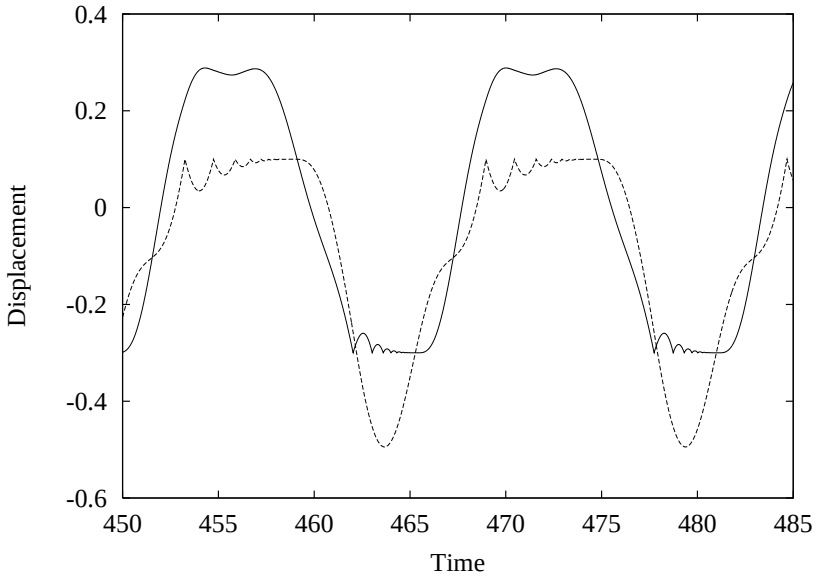
0.4
0.2
0
-0.2
-0.4
-0.6
Displacement
450
455
460
465
470
475
480
485
Time

(a)

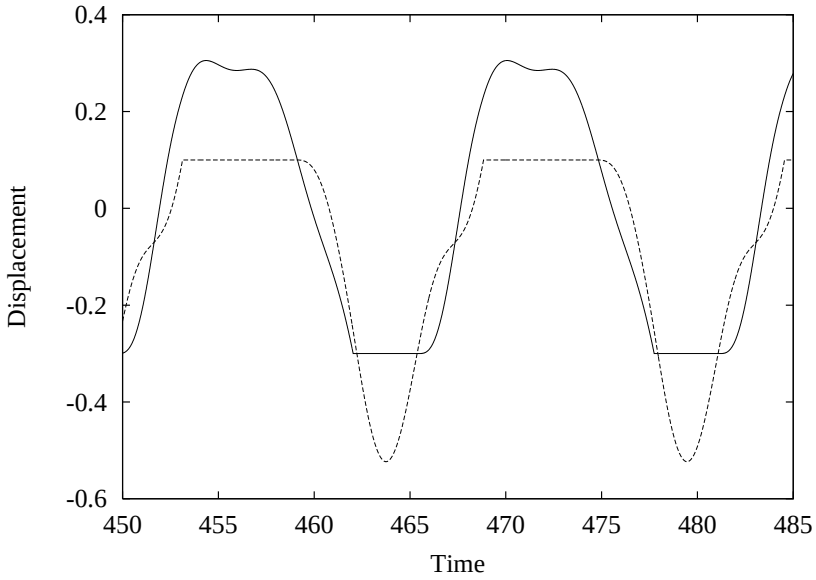
0.4
0.2
0
-0.2
-0.4
-0.6
Displacement
450
455
460
465
470
475
480
485
Time

(b)

Figure 3:

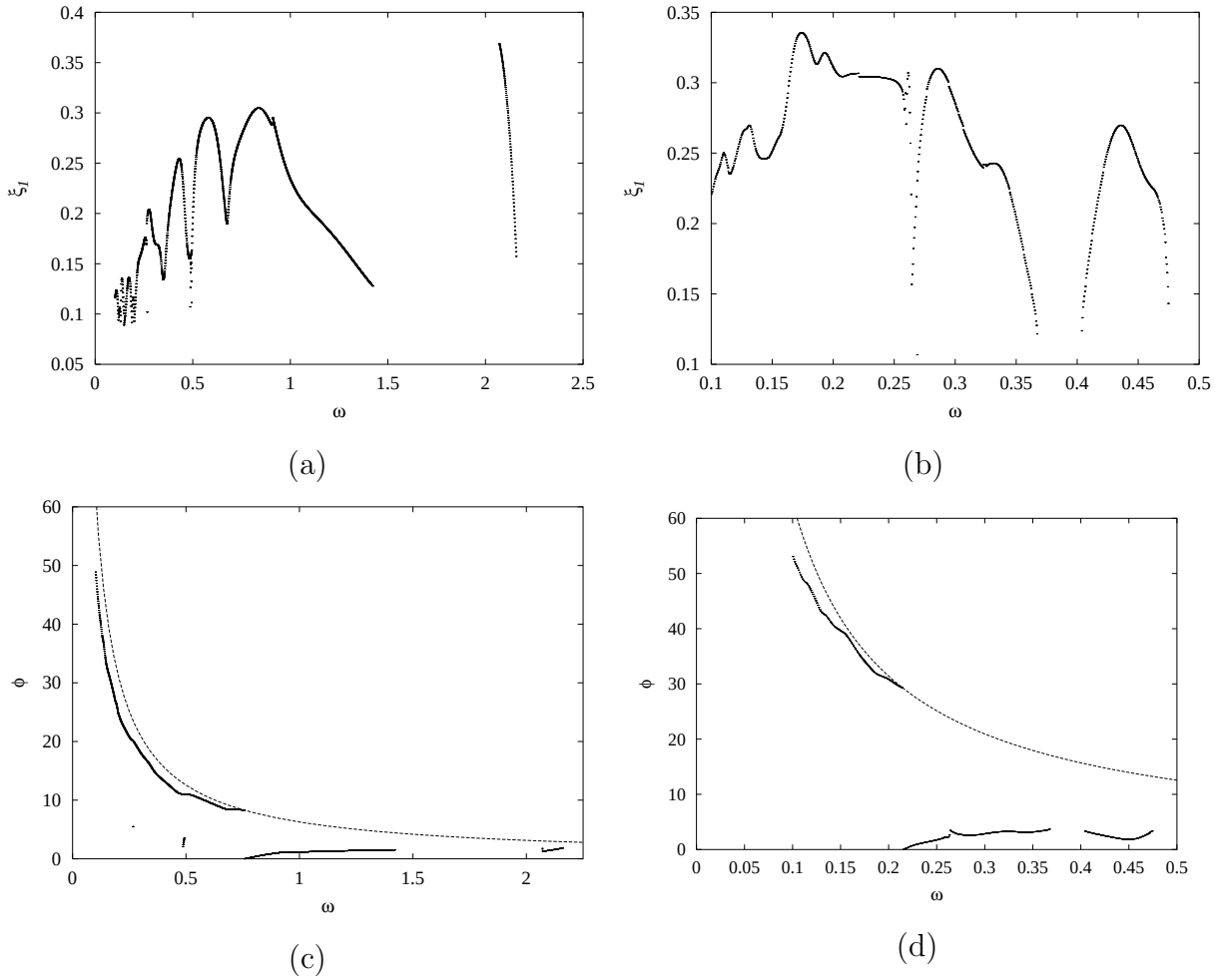

Figure 4:

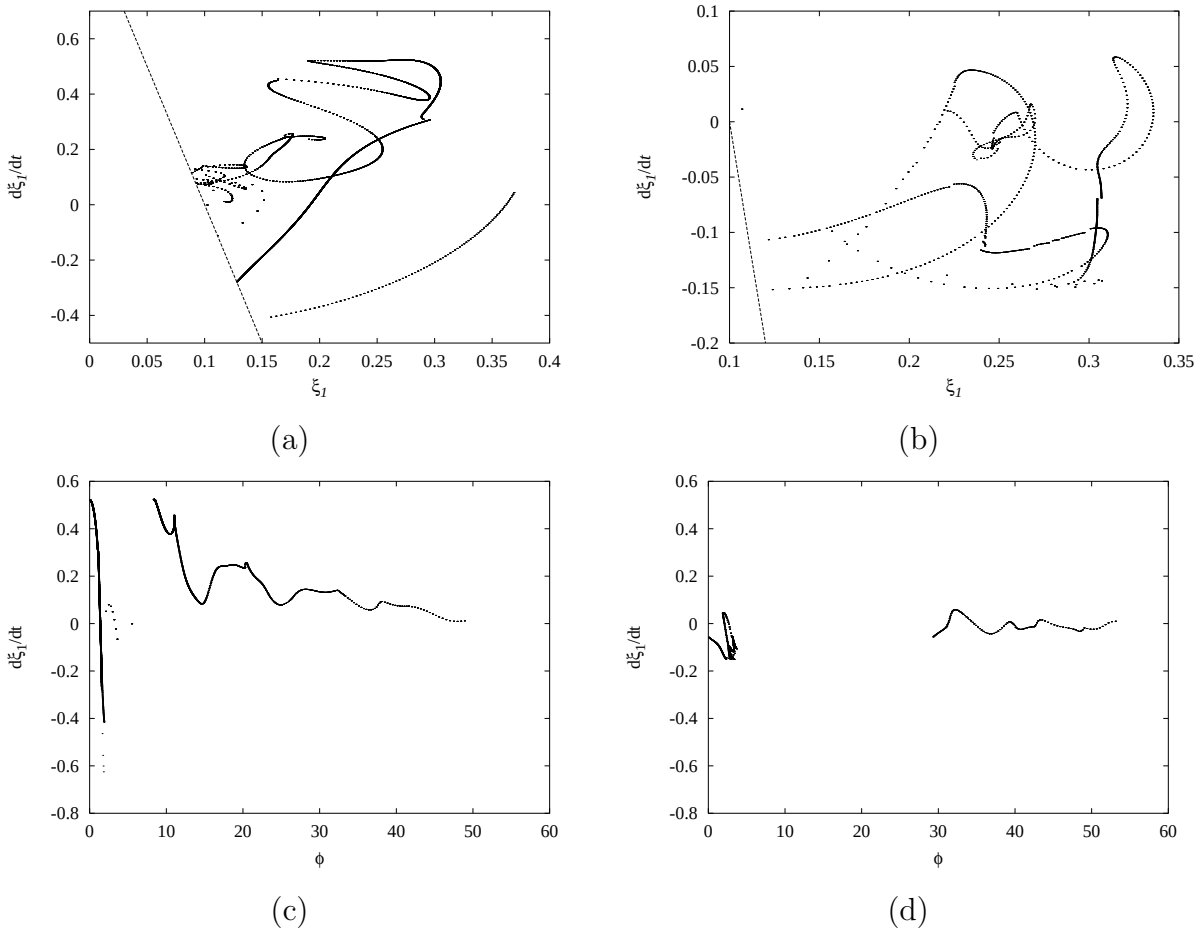

Figure 5:

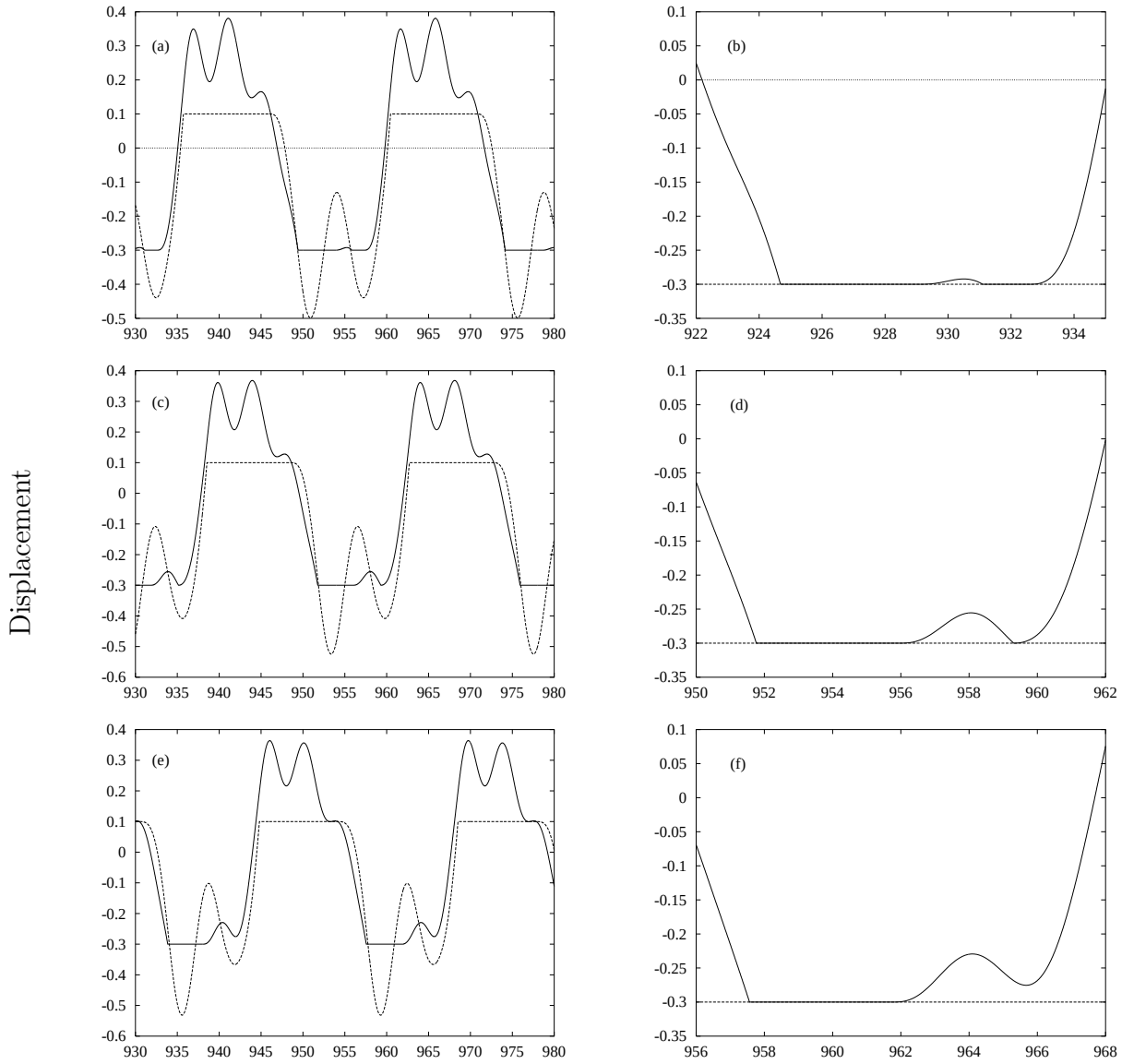

Figure 6:

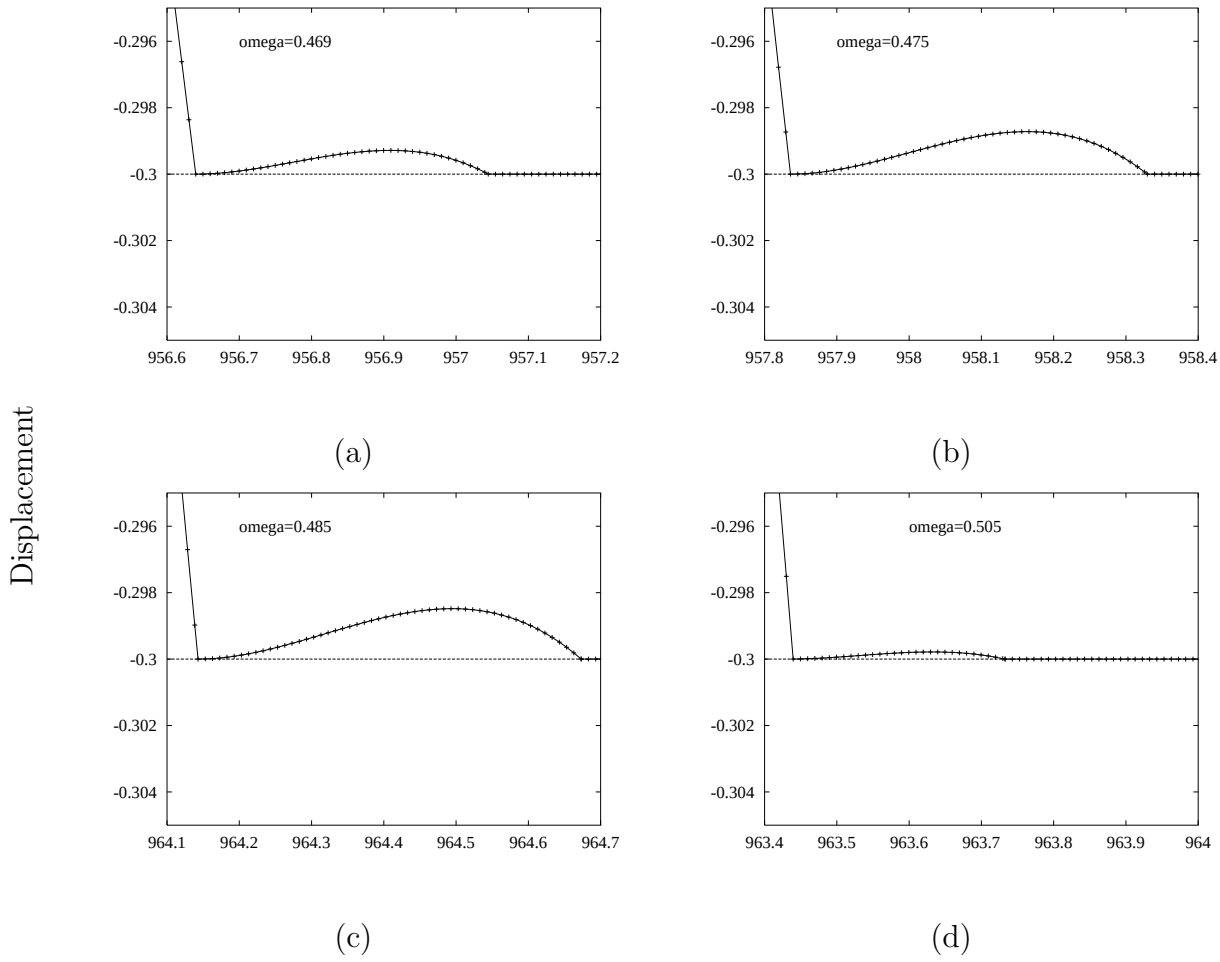
omega=0.469
omega=0.475
omega=0.485
omega=0.505
-0.296
-0.298
-0.3
-0.302
-0.304
956.6
956.7
956.8
956.9
957
957.1
957.2
957.8
957.9
958
958.1
958.2
958.3
958.4
964.1
964.2
964.3
964.4
964.5
964.6
964.7
963.4
963.5
963.6
963.7
963.8
963.9
964
(a)
(b)
(c)
(d)
Displacement
Time

Figure 7:

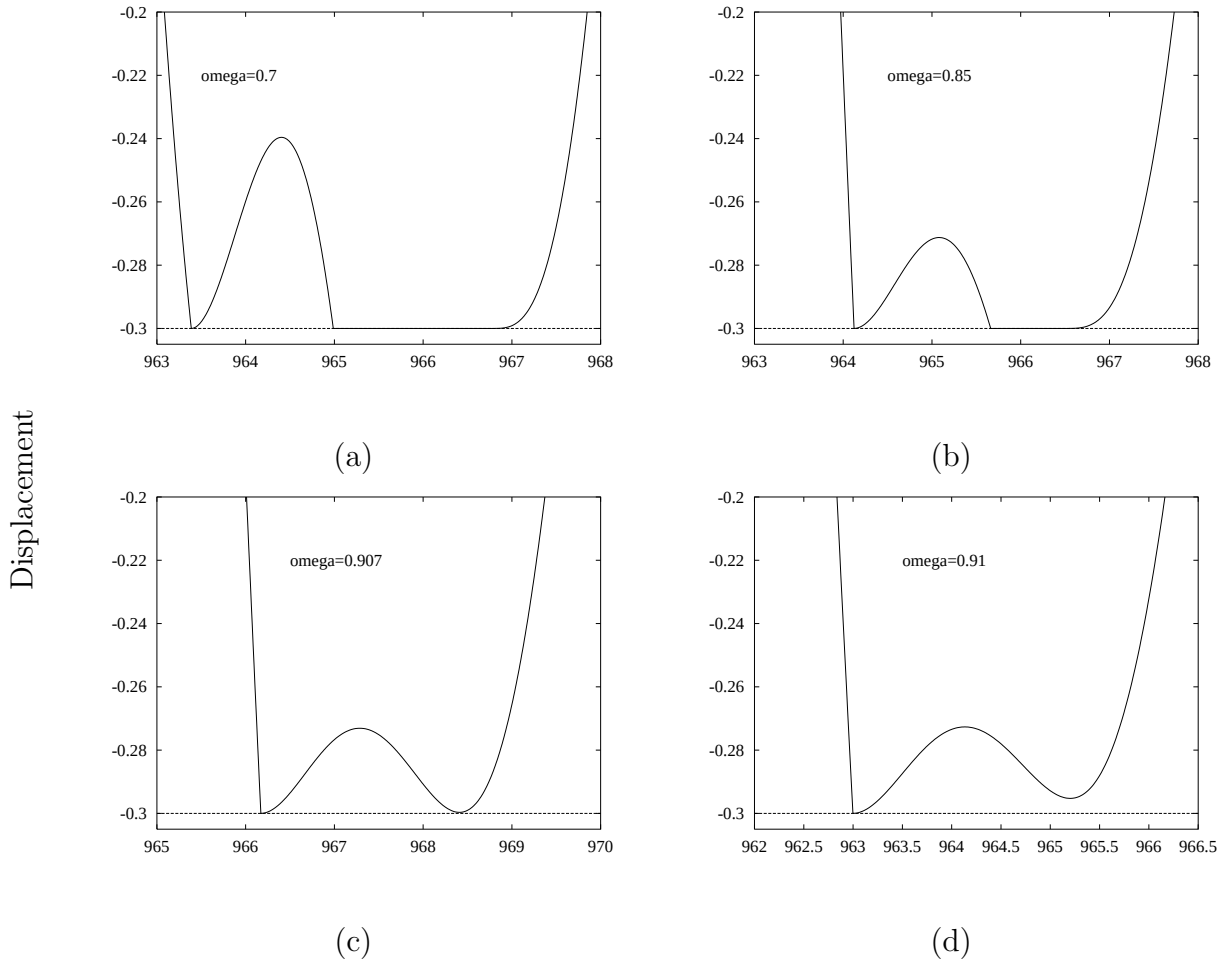
omega=0.7
omega=0.85
omega=0.907
omega=0.91
(a)
(b)
(c)
(d)
Displacement
Time

Figure 8: